

Probing Dark Matter Interactions with Stellar Motion near Sagittarius A*

R. Andrew Gustafson,^{1,2} Ian M. Shoemaker,¹ and Volodymyr Takhistov^{2,3,4,5}

¹*Center for Neutrino Physics, Department of Physics, Virginia Tech, Blacksburg, VA 24061, USA*

²*International Center for Quantum-field Measurement Systems for Studies of the Universe and Particles (QUP, WPI), High Energy Accelerator Research Organization (KEK), Oho 1-1, Tsukuba, Ibaraki 305-081, Japan*

³*Theory Center, Institute of Particle and Nuclear Studies (IPNS),*

High Energy Accelerator Research Organization (KEK), Oho 1-1, Tsukuba, Ibaraki 305-081, Japan

⁴*Graduate University for Advanced Studies (SOKENDAI), Oho 1-1, Tsukuba, Ibaraki 305-081, Japan*

⁵*Kavli Institute for the Physics and Mathematics of the Universe (WPI),*

The University of Tokyo Institutes for Advanced Study,

The University of Tokyo, Kashiwa, Chiba 277-8583, Japan

Stars orbiting Sgr A* at the Milky Way's center provide a unique laboratory to test gravity and dark matter (DM). We demonstrate that DM interactions in stellar interiors induce a novel momentum transfer force, altering orbits beyond gravitational effects. Using S2's 2000-2019 orbital data we derive the first astrophysical constraints on DM-nucleon scattering, excluding new sub-GeV parameter space. Stellar lifetime constraints over Myr timescales complement these, surpassing some direct detection and cosmological limits. This establishes stellar dynamics as a novel probe of DM interactions.

Introduction.— The Milky Way's Galactic Center provides a unique natural laboratory for testing gravity and probing the fundamental properties of dark matter (DM) - the Universe's dominant matter, detected only gravitationally thus far. Observations of S-cluster stars orbiting the Galactic Center have confirmed the presence of a supermassive black hole Sagittarius A* (Sgr A*) with mass of $M_{\text{BH}} \simeq 4 \times 10^6 M_{\odot}$ at ~ 8 kpc [1, 2]. Precision measurements of stellar motion, particularly S2, have enabled stringent tests of general relativity [3].

DM is expected to cluster around supermassive black holes due to gravity, forming overdense “spikes” that can enhance the local DM density by orders of magnitude [4–6]. These overdensities can significantly affect DM observations and signatures [6–10]. Variety of studies have explored the impact on the S-cluster stars [11–13].

Here we put forth a novel approach for probing fundamental DM interactions by considering scattering of DM particles with constituents inside stellar interiors that induce a net momentum transfer capable of altering stellar orbital motion and, over extended timescales, degrading the orbits. These effects depend simultaneously on the macroscopic DM distribution near Sgr A* and the microscopic DM scattering cross-sections. Unlike processes that rely on energy deposition, such as DM capture or annihilation, this momentum transfer mechanism remains efficient even for lighter sub-GeV DM masses. Thus, our approach provides a new bridge between stellar dynamics and dark sector particle physics.

Dark matter properties.— We denote the DM particle by χ with mass m_χ and characterize its density profile near the Galactic Center with a power-law spike [6]

$$\rho_\chi(r) = \rho_{\text{sp}} \left(\frac{R_{\text{sp}}}{r} \right)^\gamma, \quad (1)$$

where ρ_{sp} is the density at the outer spike boundary, γ is the index and R_{sp} is the spike radius. Although

the DM profile is expected to be modified within a few Schwarzschild radii of supermassive black hole due to relativistic effects [16, 17], and at distant $r \gg R_{\text{sp}}$ regions the DM halo is expected to follow characteristic distribution [18], the description is valid for the stellar orbit analysis considered here. While the exact structure and evolution of the DM spike depend on the Galactic Center's dynamical history, the adopted power law form provides a well motivated representative benchmark. We examine the effect of varying its parameters in the Supplemental Material.

The DM velocity \mathbf{v}_χ distribution is considered to be Maxwell-Boltzmann in the supermassive black hole frame. In the star's frame with velocity \mathbf{v}_s one has

$$f(\mathbf{v}_\chi) = \frac{1}{v_{\text{char}}^3 \pi^{3/2}} \exp \left(-\frac{(\mathbf{v}_\chi + \mathbf{v}_s)^2}{v_{\text{char}}^2} \right) \quad (2)$$

where $v_{\text{char}} = \sqrt{2GM_{\text{BH}}/\mathcal{F}r}$, G the gravitational constant, and the factor \mathcal{F} ranging 2.8 to 5.5 in analyses of active galactic nuclei [19–21]. We adopt $\mathcal{F} = 3.5$, finding results to not be significantly affected by this choice.

For DM interactions with Standard Model particles we focus on minimal spin-independent scattering off nucleons, with our analysis methodology readily applicable to other DM interactions. The temperature of the considered stars is sufficiently low such that we can treat the nucleons as at rest relative to DM. The differential cross-section with respect to nucleon recoil energy E_R , and momentum transfer $q = \sqrt{2m_N E_R}$ for nucleus of mass m_N , is

$$\frac{d\sigma}{dE_R} = \frac{\bar{\sigma}_n m_N}{2\mu_n^2 v_\chi^2} \left(\frac{m_V^2 + q_0^2}{m_V^2 + q^2} \right)^2 |F_N(q)|^2 \quad (3)$$

where m_V is the mediator mass, μ_n is the DM-nucleon reduced mass, $\bar{\sigma}_n$ is a characteristic cross section and

Stars	$M_s(M_\odot)$	$R_s(R_\odot)$	$a(\text{AU})$	e	$T_0(\text{yr})$	$i(^{\circ})$	$\omega(^{\circ})$	$\Omega(^{\circ})$
S2	$13.6^{+2.2}_{-1.8}$	$5.53^{+1.77}_{-0.79}$	1007 ± 1.5	0.886 ± 0.0004	2018.37 ± 0.0004	133.88 ± 0.18	66.03 ± 0.24	227.40 ± 0.29
S62	6.1^{+2}_{-1}	$4.24^{+1.08}_{-1.16}$	737 ± 4	0.976 ± 0.01	2003.33 ± 0.02	72.76 ± 5.15	42.62 ± 2.29	122.61 ± 4.01
S4711	2.2^{+2}_{-1}	$1.87^{+1.27}_{-0.72}$	616 ± 12	0.768 ± 0.03	2010.85 ± 0.06	114.71 ± 2.92	131.59 ± 3.09	20.10 ± 3.72
S4714	2.0^{+2}_{-1}	$1.74^{+1.29}_{-0.74}$	837 ± 2	0.985 ± 0.011	2017.29 ± 0.02	127.70 ± 0.28	357.25 ± 0.80	129.28 ± 0.63

TABLE I. Parameters of the S-cluster stars analyzed in this work. Values for S2 are taken from Ref. [3, 14], and those for S62, S4711, and S4714 from Ref. [15]. For stars other than S2, the radius is estimated as $R_s = R_\odot(M_s/M_\odot)^{0.8}$. The variables i , ω , and Ω denote the inclination, longitude of the pericenter and the position angle of the ascending node, respectively. T_0 is the time of closest approach to Sgr A*.

$q_0 = \mu_n v_\chi$. Here we work in natural units. For considered energies the nuclear form factor is always $F_N(q) = 1$ [22].

We define

$$\sigma_T = \int \frac{d\sigma}{dE_R} \frac{m_N E_R}{\mu^2 v_\chi^2} dE_R \quad (4)$$

and the optical depth analog $\tau_T = 2R_s n_N \sigma_T m_N / (m_\chi + m_N)$ for star of mass M_s and radius R_s and nucleon number density $n_N = (M_s/m_N)(4\pi R_s^3/3)^{-1}$. For a DM particle with velocity \mathbf{v}_χ traversing the star, the average momentum imparted to the star is

$$\langle \mathbf{p}_{\text{SM}} \rangle = m_\chi \mathbf{v}_\chi \left(1 - 2 \frac{1 - \exp(-\tau_T)(1 + \tau_T)}{\tau_T^2} \right), \quad (5)$$

with derivation found in Supplemental Material.

We find the force on the star from DM interactions is

$$\mathbf{F}_{\text{scat}} = \pi R_s^2 \frac{\rho_\chi}{m_\chi} v_s \int \langle \mathbf{p}_{\text{SM}} \rangle f(\mathbf{v}_\chi) d^3 \mathbf{v}_\chi \quad (6)$$

where $v_s = |\mathbf{v}_s|$. Eq. (5) saturates to $m_\chi \mathbf{v}_\chi$ for $\tau_T \gg 1$, yielding a maximal force scaling linearly with ρ_χ and nearly quadratically with v_s when $v_s \gg v_{\text{char}}$.

Effects on astrometric observations.— Precision measurements of S-cluster star motion, especially that of S2, provide sensitive probes of new physics including tests of general relativity [3]. We analyze the stars S2, S62, S4711 and S4714 whose relevant parameters are described in Tab. I and adopt Sgr A* properties from Ref. [3]. The principal observables are the stellar right ascension (RA), declination (Dec), and radial velocity (RV).

DM can influence these stellar orbits through three distinct mechanisms. Purely gravitational effects arise from extended mass distribution [11] and also induce dynamical friction (e.g. [12], and earlier proposed in the context of other supermassive black holes [23, 24]). Our interest is in direct DM scattering with nucleons within stellar interiors, which produces a novel non-gravitational momentum transfer force described by the formalism developed above. Among these, only the last effect directly probes DM microphysics.

To investigate the impact of these DM effects, we perform three distinct types of first post-Newtonian order orbital simulations (see Supplemental Material for details).

Namely, we consider: (i) a reference case with only supermassive black hole, (ii) a case of supermassive black hole plus a DM spike affecting the orbit solely through gravity and (iii) a case of supermassive black hole with DM spike and including DM-nucleon interactions. We then compare the simulated astrometric observables between cases (i) and (ii), corresponding to purely gravitational effects, and between (ii) and (iii), corresponding to DM scattering interaction effects. We find that dynamical friction is negligible compared to other effects across the relevant parameter space and omit it (see Supplemental Material for justification).

In Fig. 1 we display resulting differences in radial velocities considering a large cross section ($\tau_T \gg 1$), with RA and Dec found in Supplemental Material. At early times, gravity only perturbations dominate. As the star approaches pericenter, where both its velocity and the DM density are largest, the DM scattering-induced deviations rapidly grow. For highly eccentric stars such as S62 and S4714 the DM scattering effects can exceed purely gravitational contributions. Since the two effects are non-degenerate astrometric observations could disentangle them.

Using 19 years of existing S2 observational data [3] we estimate novel exclusions for DM interactions. Fixing the DM spike index γ and density at 0.01 pc we vary the DM mass and scattering cross-section. We simulate the S2 motion from 2000 to 2019 with and without scattering (see Supplemental Material). The average observational $1-\sigma$ uncertainties during this period were $\simeq 550 \mu\text{as}$ in RA/Dec and $\simeq 30 \text{ km s}^{-1}$ in RV. If the scattering effect alone produces deviations of this magnitude we consider the corresponding parameter point excluded and in the red region denoted “S2 Astrometric” of Fig. 2. Our study thus calls for dedicated analyses by experimental collaborations that can further improve on our results.

Near future experiments will be able to probe DM interactions with significantly enhanced sensitivity. We project their reach by considering that future astrometric precision of $\simeq 100 \mu\text{as}$ in RA/Dec and $\simeq 10 \text{ km s}^{-1}$ in RV, consistent with GRAVITY [25], the Thirty Meter Telescope [26], NIFS [27] and OSIRIS [28]. We consider DM parameter points yielding such deviations within a 20-year observational period as detectable.

As shown in Fig. 2, the exclusion limits we estimated

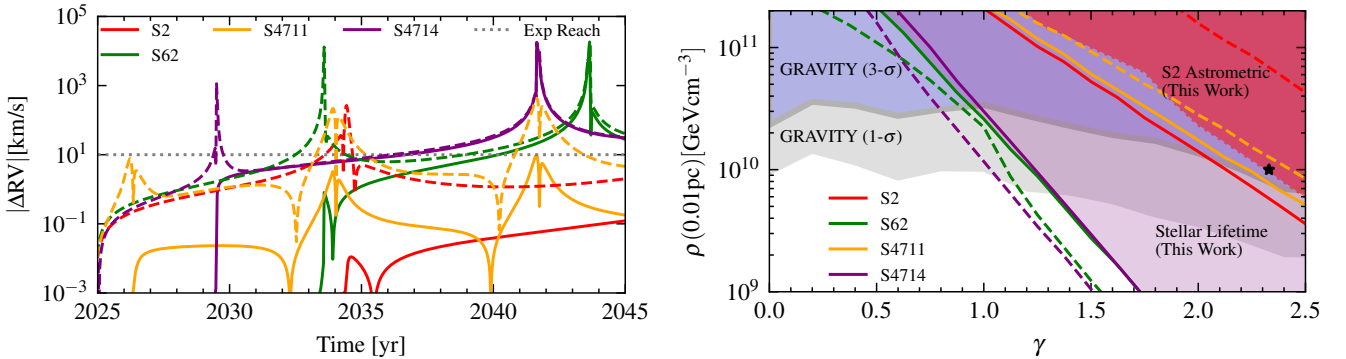


FIG. 1. **Left:** RV deviations induced by DM obtained from our simulations. Dashed lines indicate the difference between a stellar orbit without a DM overdensity spike and one with a spike and only gravitational interactions. Solid lines indicate the difference between two orbits with DM spikes with and without DM-nucleon scattering. We consider a characteristic DM spike profile with $\gamma = 7/3$, $\rho(0.01\text{pc}) = 10^{10} \text{ GeV cm}^{-3}$ as well as $\tau_T \gg 1$ for DM scattering. The dotted horizontal line indicates the reach of 10 km s^{-1} for near future astrometric measurements [3, 25–28]. **Right:** DM density at 0.01 pc versus spike index for $m_\chi = 10^{-2} \text{ GeV}$ and $\sigma_n = 5 \times 10^{-35} \text{ cm}^2$ with a heavy mediator. Solid lines denote tidal disruption events within 1 Myr, the purple shaded region indicates parameters where any of the four stars would undergo a tidal disruption. Dashed lines correspond to observational sensitivities of 10 km s^{-1} or 0.1 mas . The red region denotes where DM scattering effects on S2 in 2000–2019 data cause deviations exceeding measurement uncertainties [3]. The 1- σ and 3- σ gravitational only exclusions from GRAVITY [11] are shown. The black star indicates the parameters used in Fig. 2.

for S2 considering 2000–2019 data exceeds the expected sensitivity (dashed lines) from future observations of S2 between 2025 and 2045. While the upcoming observations carry improved precision, S2 passed through pericenter twice during 2000–2019 period but will do so only once in 2025–2045 period. Since DM scattering effects peak at the pericenter, stars with larger eccentricities and smaller pericenter distances provide strongest constraints on DM interactions. This highlights the significance of multi-decade observations of these stars, as each pass through the pericenter leads to compounding effects.

Effects on stellar lifetimes.— DM can impact long-term survival of stars by inducing orbital energy losses and decay. While minuscule on human timescales, dynamical processes near supermassive black hole are expected to act over $\mathcal{O}(10^6)$ yr [37]. Thus, we impose new indirect limits on DM interactions by requiring that stellar orbits remain stable for at least this timescale.

Among the possible mechanisms both dynamical friction and DM scattering lead to energy losses. A static ex-

tended mass distribution only modifies the gravitational potential without dissipating energy. Thus, DM scattering processes are dominant contributions to stellar orbital evolution in our analysis.

We define the end of the stellar lifetime when the star crosses its tidal disruption event radius $r_{\text{TDE}} = (M_{\text{BH}}/M_s)^{1/3} R_s$. Due to slowly varying changes we average the evolution over many Keplerian orbits for which the orbital position and velocity depend on the true anomaly f , semimajor axis a and eccentricity e as

$$r(f) = \frac{a(1-e^2)}{(1+e\cos(f))} \quad , \quad \frac{df}{dt} = \frac{n(1+e\cos(f))^2}{(1-e^2)^{3/2}} \quad , \quad (7)$$

with $n = \sqrt{GM_{\text{BH}}/a^3}$. Following Ref. [38, 39], we introduce a dimensionless function $\epsilon(r, v_s)$ such that

$$\epsilon(r, v_s) \mathbf{v}_s = -\frac{\mathbf{F} v_s^3}{M_s} \quad (8)$$

where \mathbf{F} is the total force acting on the star.

Averaging over many orbital periods yields parameter evolution equations [38, 39]

$$\left\langle \frac{da}{dt} \right\rangle = \frac{(1-e^2)^2}{\pi n^3 a^2} \int_0^{2\pi} \frac{(1+e\cos(f))^{-2} \epsilon(r, v_s)}{(1+e^2+2e\cos(f))^{1/2}} df \quad , \quad (9)$$

$$\left\langle \frac{de}{dt} \right\rangle = \frac{(1-e^2)^3}{\pi n^3 a^3} \int_0^{2\pi} \frac{(e+\cos(f)) \epsilon(r, v_s)}{(1+e^2+2e\cos(f))^{3/2} (1+e\cos(f))^2} df \quad . \quad (10)$$

Using the present day orbital parameters in Tab. I we

determine the orbital evolution. We exclude DM param-

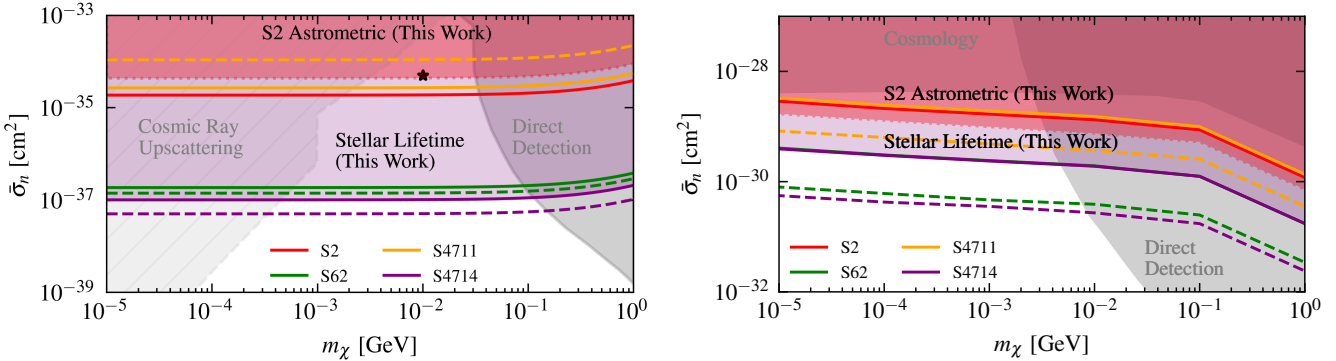


FIG. 2. DM-nucleon scattering cross-section versus DM mass for a heavy mediator (**left**) and a light mediator with $m_V = 1$ eV (**right**). A characteristic DM overdensity spike index of $\gamma = 7/3$ and density $\rho(0.01\text{pc}) = 10^{10} \text{ GeV cm}^{-3}$ is considered. The red region denotes where DM scattering effects on S2 in 2000-2019 data cause deviations exceeding measurement uncertainties [3]. Solid lines mark tidal disruption events within 1 Myr, the purple region indicating parameters where any of the four stars would undergo a tidal disruption. Dashed lines correspond to deviations of 10 km s^{-1} in RV or $100 \mu\text{as}$ in RA or Dec over 20 yr period, comparable to current and near future sensitivities [3, 25-28]. Limits from direct detection from SENSEI, XENON, LUX, and PandaX [29-33] as well as cosmological constraints [34] that include CMB with BAO, Lyman- α forest and Milky Way satellite measurements are shown. We also display cosmic-ray boosted DM bound estimates for IceCube [35] and limits from Super-Kamiokande [36], indicated with hatched contours and dashed lines reflecting their additional model dependence and complementarity. The black star in the left panel marks parameters used in Fig. 1.

eters that result in tidal disruption events within 1 Myr, shorter than the stellar lifetime [14] or other dynamical processes near Sgr A* [37]. This constrains the DM profile overdensity and slope for a given DM mass and cross-section, as shown in Fig. 1. Equivalently, this restricts the DM interaction parameters for fixed DM overdensity profile properties as shown on Fig. 2 by the purple “Stellar Lifetime” region that denotes the parameter space where any of the four stars S2, S62, S4711, S4714 would be disrupted within 1 Myr.

The constraint’s dependence on the on the scattering optical depth τ_T , as used in Eq. (5), illustrates effects of imposing alternative stellar lifetime restrictions. If $\tau_T \ll 1$ then stellar lifetime scales as $\tau_T^{-1} \propto \sigma_n^{-1}$, while for $\tau_T \gtrsim 1$ the stellar lifetime saturates and further increases in the cross-section do not shorten the time to disruption.

Conclusions.— We have established a previously overlooked mechanism through which DM interactions within stellar interiors induce a net momentum transfer that can significantly alter stellar motion around the Galactic Center supermassive black hole Sgr A*. This effect directly links the microphysics of DM interactions to the macroscopic orbital dynamics of stars and can exceed purely gravitational perturbations. Applying this framework to the decades-long orbital observations of the S2 star we set first astrophysical limits on DM-nucleon scattering cross-sections derived from stellar dynamics, excluding previously underexplored parameter space by more than an order of magnitude. The predicted signatures depend on orbital eccentricity and pericenter distances, making eccentric S-cluster stars the most sensitive probes of DM overdensities near the black hole.

Requiring stellar survival over Myr-timescales yields independent and complementary constraints exceeding cosmological and direct detection bounds by orders of magnitude for considered DM distributions.

Our results establish stellar dynamics near Sgr A* as a new sensitive laboratory for testing dark sector interactions and motivate future high precision astrometric campaigns that will probe DM microphysics in extreme gravitational environments.

Note added:— During the final stages of this work a preprint appeared [40] that also considered DM scattering effects and impact on Galactic Center orbits. Our analysis offers several essential advances and provides a complementary perspective: we derive the first constraints based on existing decades-long S2 astrometric data, perform full orbital simulations including scattering dynamics, present 20 year observational projections and develop a novel formalism for long term evolution.

Acknowledgments.— We are grateful to Wick Haxton and Gonzalo Herrera for useful discussions. R.A.G. and I.M.S. are supported by the U.S. Department of Energy under the award number DE-SC0020262. R.A.G. is partially supported by the World Premier International Research Center Initiative (WPI), MEXT, Japan. R.A.G. is grateful to QUP for hospitality during his visit. V.T. acknowledges support by the World Premier International Research Center Initiative (WPI), MEXT, Japan and JSPS KAKENHI grant No. 23K13109. This material is based upon work supported by the U.S. Department of Energy, Office of Science, Office of Workforce Development for Teachers and Scientists, Office of

Science Graduate Student Research (SCGSR) program. The SCGSR program is administered by the Oak Ridge Institute for Science and Education (ORISE) for the DOE. ORISE is managed by ORAU under contract number DESC0014664. R.A.G. is a recipient of the SCGSR Award.

[1] A. M. Ghez, B. L. Klein, M. Morris, and E. E. Becklin, *Astrophys. J.* **509**, 678 (1998), arXiv:astro-ph/9807210.

[2] A. Eckart and R. Genzel, *Nature* **383**, 415 (1996).

[3] T. Do *et al.*, *Science* **365**, 664 (2019), arXiv:1907.10731 [astro-ph.GA].

[4] P. Peebles, *General Relativity and Gravitation* **3**, 63 (1972).

[5] G. D. Quinlan, L. Hernquist, and S. Sigurdsson, arXiv preprint astro-ph/9407005 (1994).

[6] P. Gondolo and J. Silk, *Phys. Rev. Lett.* **83**, 1719 (1999), arXiv:astro-ph/9906391.

[7] O. Y. Gnedin and J. R. Primack, *Phys. Rev. Lett.* **93**, 061302 (2004), arXiv:astro-ph/0308385.

[8] G. Bertone, G. Sigl, and J. Silk, *Mon. Not. Roy. Astron. Soc.* **337**, 98 (2002), arXiv:astro-ph/0203488.

[9] H. Nishikawa, E. D. Kovetz, M. Kamionkowski, and J. Silk, *Phys. Rev. D* **99**, 043533 (2019), arXiv:1708.08449 [astro-ph.CO].

[10] Q. Ding, M. He, and V. Takhistov, *Astrophys. J.* **981**, 62 (2025), arXiv:2410.02591 [astro-ph.CO].

[11] K. Abd El Dayem *et al.* (GRAVITY), *Astron. Astrophys.* **692**, A242 (2024), arXiv:2409.12261 [astro-ph.GA].

[12] G. M. Tomaselli and A. Caputo, (2025), arXiv:2509.03568 [astro-ph.GA].

[13] I. John, R. K. Leane, and T. Linden, *Phys. Rev. D* **109**, 123041 (2024), arXiv:2311.16228 [astro-ph.HE].

[14] M. Habibi, S. Gillessen, F. Martins, F. Eisenhauer, P. Plewa, O. Pfuhl, E. George, J. Dexter, I. Waisberg, T. Ott, *et al.*, *The Astrophysical Journal* **847**, 120 (2017).

[15] F. Peišker, A. Eckart, M. Zajaček, B. Ali, and M. Parsa, *The Astrophysical Journal* **899**, 50 (2020).

[16] L. Sadeghian, F. Ferrer, and C. M. Will, *Phys. Rev. D* **88**, 063522 (2013), arXiv:1305.2619 [astro-ph.GA].

[17] N. Speeney, A. Antonelli, V. Baibhav, and E. Berti, *Phys. Rev. D* **106**, 044027 (2022), arXiv:2204.12508 [gr-qc].

[18] J. F. Navarro, C. S. Frenk, and S. D. M. White, *Astrophys. J.* **462**, 563 (1996), arXiv:astro-ph/9508025.

[19] C. A. Onken, L. Ferrarese, D. Merritt, B. M. Peterson, R. W. Pogge, M. Vestergaard, and A. Wandel, *Astrophys. J.* **615**, 645 (2004), arXiv:astro-ph/0407297.

[20] A. Pancoast, B. J. Brewer, T. Treu, D. Park, A. J. Barth, M. C. Bentz, and J.-H. Woo, *Mon. Not. Roy. Astron. Soc.* **445**, 3073 (2014), arXiv:1311.6475 [astro-ph.CO].

[21] B. Peterson, C. Grier, K. Horne, R. Pogge, M. Bentz, G. De Rosa, K. Denney, P. Martini, S. Sergeev, S. Kaspi, *et al.*, *The Astrophysical Journal* **795**, 149 (2014).

[22] I. Angeli, *Atomic Data and Nuclear Data Tables* **87**, 185 (2004).

[23] M. H. Chan and C. M. Lee, *Astrophys. J. Lett.* **962**, L40 (2024), arXiv:2402.03751 [astro-ph.GA].

[24] Q. Ding, M. He, V. Takhistov, and H.-Y. Zhu, (2025), arXiv:2505.09696 [hep-ph].

[25] R. Abuter, A. Amorim, M. Bauböck, J. Berger, H. Bonnet, W. Brandner, Y. Clénet, R. Davies, P. de Zeeuw, J. Dexter, *et al.*, *Astronomy & Astrophysics* **647**, A59 (2021).

[26] S. Yelda, L. Meyer, A. Ghez, and T. Do, arXiv preprint arXiv:1310.5744 (2013).

[27] P. J. McGregor, J. Hart, P. G. Conroy, M. L. Pfitzner, G. J. Bloxham, D. J. Jones, M. D. Downing, M. Dawson, P. Young, M. Jarnyk, and J. V. Harmelen, in *Instrument Design and Performance for Optical/Infrared Ground-based Telescopes*, Vol. 4841, edited by M. Iye and A. F. M. Moorwood, International Society for Optics and Photonics (SPIE, 2003) pp. 1581 – 1591.

[28] A. Quirrenbach, J. E. Larkin, A. Krabbe, M. Barczys, and D. LaFreniere, in *Instrument Design and Performance for Optical/Infrared Ground-based Telescopes*, Vol. 4841, edited by M. Iye and A. F. M. Moorwood, International Society for Optics and Photonics (SPIE, 2003) pp. 1493 – 1502.

[29] L. Barak *et al.* (SENSEI), *Phys. Rev. Lett.* **125**, 171802 (2020), arXiv:2004.11378 [astro-ph.CO].

[30] P. Adari *et al.* (SENSEI), *Phys. Rev. Lett.* **134**, 011804 (2025), arXiv:2312.13342 [astro-ph.CO].

[31] R. Essig, J. Pradler, M. Sholapurkar, and T.-T. Yu, *Phys. Rev. Lett.* **124**, 021801 (2020), arXiv:1908.10881 [hep-ph].

[32] D. S. Akerib *et al.* (LUX), *Phys. Rev. Lett.* **122**, 131301 (2019), arXiv:1811.11241 [astro-ph.CO].

[33] X. Ren *et al.* (PandaX-II), *Phys. Rev. Lett.* **121**, 021304 (2018), arXiv:1802.06912 [hep-ph].

[34] M. A. Buen-Abad, R. Essig, D. McKeen, and Y.-M. Zhong, *Phys. Rept.* **961**, 1 (2022), arXiv:2107.12377 [astro-ph.CO].

[35] C. V. Cappiello, Q. Liu, G. Mohlabeng, and A. C. Vincent, *Phys. Rev. D* **110**, 095031 (2024), arXiv:2405.00086 [hep-ph].

[36] K. Abe *et al.* (Super-Kamiokande), *Phys. Rev. Lett.* **130**, 031802 (2023), [Erratum: *Phys. Rev. Lett.* 131, 159903 (2023)], arXiv:2209.14968 [hep-ex].

[37] T. Alexander, *Ann. Rev. Astron. Astrophys.* **55**, 17 (2017), arXiv:1701.04762 [astro-ph.GA].

[38] F. Dosopoulou and F. Antonini, *Astrophys. J.* **840**, 31 (2017), arXiv:1611.06573 [astro-ph.GA].

[39] F. Dosopoulou, *Phys. Rev. D* **110**, 083027 (2024), arXiv:2305.17281 [astro-ph.HE].

[40] J. F. Acevedo, A. J. Reilly, and L. Santos-Olmsted, (2025), arXiv:2510.01320 [hep-ph].

[41] S. Chandrasekhar, *Astrophys. J.* **97**, 255 (1943).

Supplemental Material for
Probing Dark Matter Interactions with Stellar Motion near Sagittarius A*

R. Andrew Gustafson, Ian M. Shoemaker, Volodymyr Takhistov

In this Supplemental Material we provide additional details on the derivation of the momentum transfer formalism for DM-nucleon scattering, the description of orbital simulations and observables, the comparative analysis of other orbital energy loss processes and supplementary figures illustrating DM-spike parameters and stellar-orbit evolution.

A. Dark Matter Scattering Momentum Transfer Formalism

We detail here the derivation of the momentum transfer induced by DM-nucleon scattering. Consider a nucleon initially at rest and a DM particle with non-relativistic velocity v_χ . After scattering the nucleon recoils with energy E_R and the outgoing DM is deflected by an angle θ . From kinematics one has

$$m_N E_R = (E_i E_f - p_i p_f \cos \theta - m_\chi^2) \quad (11)$$

where E_i and $E_f = E_i - E_R$ is the initial and final DM particle energies with corresponding initial momentum $p_i = \sqrt{E_i^2 - m_\chi^2}$ and analogously a final momentum p_f . In the non-relativistic limit

$$\frac{p_f \cos \theta}{p_i} \simeq 1 - \frac{E_R(m_N + m_\chi)}{m_\chi^2 v_\chi^2}. \quad (12)$$

Thus, the average fraction of momentum retained in the initial direction after a single scattering is

$$\left\langle \frac{p_f \cos \theta}{p_i} \right\rangle = 1 - \frac{m_N}{(m_\chi + m_N)} \frac{\sigma_T}{\sigma}, \quad (13)$$

where σ is the total cross-section and σ_T is defined in Eq. (4).

We consider that scattering does not significantly alter the DM speed, such that σ_T remains constant along the particle's path. This approximation remains accurate until $m_\chi \simeq m_N$, where direct detection limits dominate. The average momentum imparted to the star is then

$$\langle \mathbf{p}_{\text{SM}} \rangle = m_\chi \mathbf{v}_\chi \left[1 - \sum_{k=0}^{\infty} p(k) \left(1 - \frac{m_N}{(m_\chi + m_N)} \frac{\sigma_T}{\sigma} \right)^k \right], \quad (14)$$

where $p(k)$ is the probability that the DM undergoes k scatterings while traversing the star.

Assuming a uniform nucleon number density n_N and straight line DM trajectories, a conservative choice that underestimates the rates, we obtain

$$p(k) = \int_0^{R_s} dR \frac{2R \exp(-2n_N \sigma \sqrt{R_s^2 - R^2}) (2n_N \sigma \sqrt{R_s^2 - R^2})^k}{R_s^2 k!}. \quad (15)$$

Substituting into Eq. (14) and summing over k yields

$$\langle \mathbf{p}_{\text{SM}} \rangle = m_\chi \mathbf{v}_\chi \left[1 - \int_0^{R_s} dR \frac{2R}{R_s^2} \exp \left(-\frac{2m_N}{m_\chi + m_N} n_N \sigma_T \sqrt{R_s^2 - R^2} \right) \right]. \quad (16)$$

Employing optical depth analog $\tau_T = 2R_s n_N \sigma_T m_N / (m_\chi + m_N)$ as in the main text, we obtain

$$\langle \mathbf{p}_{\text{SM}} \rangle = m_\chi \mathbf{v}_\chi \left[1 - \int_0^{R_s} dR \frac{2R}{R_s^2} \exp \left(-\tau_T \sqrt{1 - \frac{R^2}{R_s^2}} \right) \right]. \quad (17)$$

Evaluating the integral gives the expression of the main text

$$\langle \mathbf{p}_{\text{SM}} \rangle = m_\chi \mathbf{v}_\chi \left(1 - 2 \frac{1 - \exp(-\tau_T)(1 + \tau_T)}{\tau_T^2} \right). \quad (18)$$

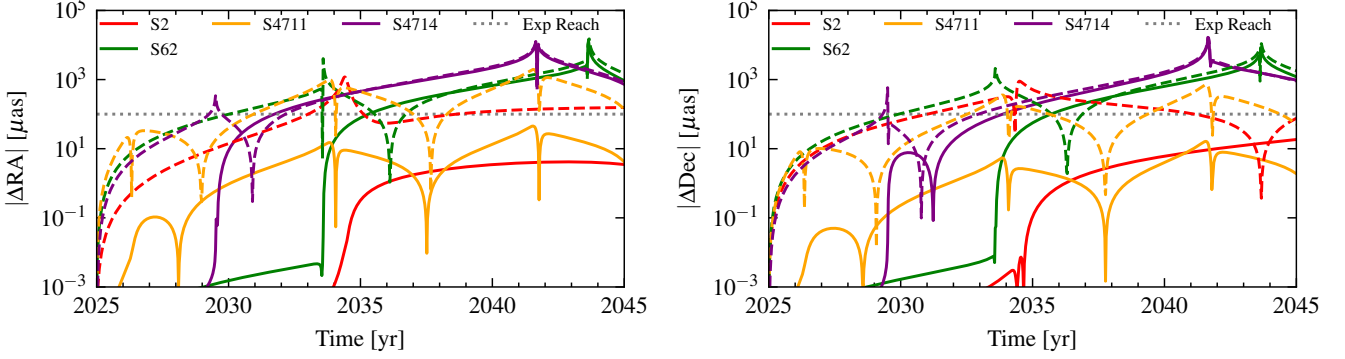


FIG. 3. Same as the left panel of Fig. 1, but showing the differences in RA (left) and Dec (right). A characteristic DM overdensity spike index of $\gamma = 7/3$ and density $\rho(0.01\text{pc}) = 10^{10} \text{ GeV cm}^{-3}$ is considered. Dashed lines denote purely gravitational effects, while solid lines include DM induced scattering.

B. Simulations of Stellar Orbits with Dark Matter Interactions

Our orbital simulations build upon the framework outlined in Ref. [3], with key modifications to incorporate DM scattering effects.

The stellar motion is computed using the first order post-Newtonian expansion, with $M_{\text{enc}}(r)$ denoting the total enclosed mass within radius r . We account for both the supermassive black hole and the DM spike. We introduce an additional non-gravitational force term \mathbf{F}_{scat} representing the DM-nucleon scattering momentum transfer effects derived in Sec. A. The full equation of motion is

$$\frac{d^2\mathbf{r}}{dt^2} = -\frac{GM_{\text{enc}}(r)\mathbf{r}}{r^3} + \frac{GM_{\text{enc}}(r)}{c^2r^3} \left(\frac{4GM_{\text{enc}}(r)}{r} - v^2 \right) \mathbf{r} + \frac{4GM_{\text{enc}}(r)(\mathbf{r} \cdot \mathbf{v})}{c^2r^3} \mathbf{v} + \frac{\mathbf{F}_{\text{scat}}}{M_s}, \quad (19)$$

where we have explicitly added back in factors of speed of light c for clarity in this section. We obtain the initial conditions using the stellar parameters in Tab. I. When modeling observables, we include the Römer time delay from light propagation

$$t_{\text{em}} \simeq t_{\text{obs}} - \frac{Z(t_{\text{obs}})}{c}, \quad (20)$$

where t_{em} is the emission time corresponding to the observed time t_{obs} and line-of-sight distance $Z(t)$. An iterative approach can further refine this relation. The emission time is then used to determine the astrometric variables.

The observed RV derived spectroscopically includes both special-relativistic and general-relativistic corrections. It relates to the true stellar velocity components (V_X, V_Y, V_Z) , defined in the observer's coordinate frame with Z along the line-of-sight, as

$$\text{RV}(t_{\text{obs}}) = V_Z(t_{\text{em}}) + \frac{V_X^2(t_{\text{em}}) + V_Y^2(t_{\text{em}}) + V_Z^2(t_{\text{em}})}{2c} + \frac{GM_{\text{enc}}(r)}{cr(t_{\text{em}})}. \quad (21)$$

Small potential offsets in Sgr A*'s position or velocity have negligible effect on differential comparisons between simulated orbits we consider.

We computed trajectories with and without the DM scattering term to isolate its influence. RV differences are shown in the main text, while changes in RA and Dec appear in Fig. 3. The DM-induced modulation of S2's RV between 2000 and 2019, used to set exclusion limits in the main text using data from Ref. [3], is shown in Fig. 4.

C. Other Energy Loss Mechanisms

The gravitational influence of an r -dependent enclosed mass can appreciably modify short term stellar observables, as depicted on Fig. 1. However, this process does not dissipate orbital energy and thus does not affect stellar lifetimes. The lowest order dissipative mechanisms arising solely from gravity are dynamical friction and gravitational wave emission. As we discuss below, both are subdominant to the DM scattering-induced effects for the stellar and DM parameters we consider. We therefore neglect them in the main analysis.

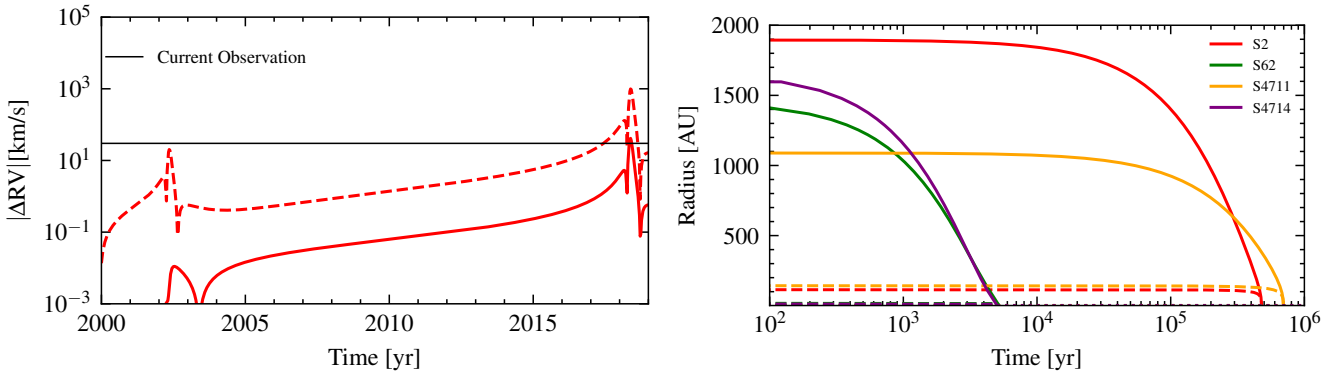


FIG. 4. **Left:** Graph of the gravitational (dashed line) and scattering induced effects (solid line) on S2 radial velocity between 2000 and 2019. The horizontal line is the average uncertainty on the radial velocity measurements during this time from [3]. **Right:** Range of the stellar radii as a function of time considering the energy loss due to scattering of DM within the spike. A characteristic DM overdensity spike index of $\gamma = 7/3$ and density $\rho(0.01\text{pc}) = 10^{10} \text{ GeV cm}^{-3}$ is considered. Solid lines indicate the apocenter distance, while dashed lines indicate the pericenter distance.

Dynamical Friction

Dynamical friction describes the deceleration of a massive body moving through a background medium due to the gravitational wake it induces [39, 41]. For an object of mass m , the dynamical friction force is given as

$$\mathbf{F}_{\text{df}} = -4\pi G^2 m \rho(r) \frac{\mathbf{v}_s}{v_s^3} \int d^3 \mathbf{v}_\chi f(\mathbf{v}_\chi) \left(\ln \Lambda \Theta(v_s - v_\chi) + \left[\ln \left(\frac{v_\chi + v_s}{v_\chi - v_s} \right) - \frac{2v_s}{v_\chi} \right] \Theta(v_\chi - v_s) \Theta(v_{\text{esc}} - v_\chi) \right) \quad (22)$$

where non-bold quantities denote magnitudes and \mathbf{v}_s is the DM velocity distribution in the supermassive black hole frame where it is isotropic. The escape velocity is $v_{\text{esc}} = \sqrt{2GM_{\text{BH}}/r}$, and $\ln \Lambda \sim \mathcal{O}(10)$ is the Coulomb logarithm. We have verified that the term in square brackets is always smaller than $\ln \Lambda$ and can be ignored.

Assuming a Maxwell–Boltzmann distribution as in Eq. (2), we can solve the force exactly as

$$\mathbf{F}_{\text{df}} = -4\pi G^2 m \rho(r) \ln \Lambda \frac{\mathbf{v}_s}{v_s^3} \left(\text{erf} \left(\frac{v_s}{v_{\text{char}}} \right) - \frac{2v_s \exp \left(-\frac{v_s^2}{v_{\text{char}}^2} \right)}{v_{\text{char}} \sqrt{\pi}} \right). \quad (23)$$

For $v_s \gg v_{\text{char}}$ the dynamical friction force scales as $\mathbf{F}_{\text{df}} \propto v_s^{-2}$ in contrast to DM scattering force $\mathbf{F}_{\text{scat}} \propto v_s^2$. This opposite scaling explains why scattering dominates for the high velocity S-cluster stars. The corresponding changes in the orbital parameters are obtained by substituting $\epsilon(r, v_s)$ from Eq. (8) into Eqs. (9) and (10).

Gravitational Waves

At small pericenter distances near the supermassive black hole stars lose orbital energy through the emission of gravitational waves leading to changes in their orbital parameters [39]. The evolution of the semimajor axis and eccentricity is given by

$$\begin{aligned} \left\langle \frac{da}{dt} \right\rangle_{\text{GW}} &= \frac{-64G^3 m M_{\text{BH}}^2}{5c^5 a^3 (1 - e^2)^{7/2}} \left(1 + \frac{73}{24} e^2 + \frac{37}{96} e^4 \right), \\ \left\langle \frac{de}{dt} \right\rangle_{\text{GW}} &= \frac{-304G^3 m M_{\text{BH}}^2}{15c^5 a^4 (1 - e^2)^{5/2}} \left(1 + \frac{121}{204} e^4 \right). \end{aligned} \quad (24)$$

In Fig. 5 we compare the relative strength of the energy loss mechanisms by considering the values of a and e for which each effect is dominant. DM scattering effects dominate in the parameter region relevant for all four stars considered in our analysis, while gravitational wave emission becomes significant only for very small pericenters, and dynamical friction is important in the opposite, low velocity limit. The transitions between these regimes are gradual.

In Fig. 4, right, we illustrate the cumulative effect of this energy loss over long timescales, showing the time evolution of the pericenter and apocenter radii induced by DM scattering.

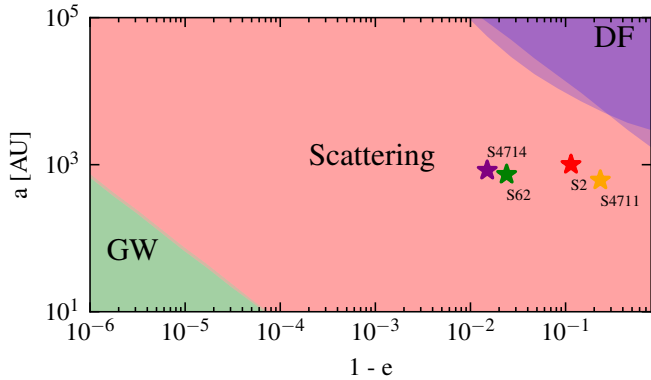


FIG. 5. Dominant contribution to the orbital evolution of the semimajor axis a and eccentricity e , as a function of a and e , comparing DM scattering, gravitational wave (GW) emission and dynamical friction (DF). We consider DM with a mass $m_\chi = 10^{-2}$ GeV with a cross section of $\sigma_n = 1.37 \times 10^{-36}$ cm 2 . A characteristic DM overdensity spike index of $\gamma = 7/3$ and density $\rho(0.01\text{pc}) = 10^{10}$ GeV cm $^{-3}$ is considered. For this comparison we consider a star with solar mass and radius. The locations of the four S-cluster stars analyzed in this work are also indicated.

D. Dependence on Dark Matter Distribution

As discussed in the main text, the sensitivity of our analysis depends jointly on the DM microphysical interactions through the scattering cross-section and the macrophysical properties of the central DM overdensity spike distribution. Since these quantities carry some degeneracy, variations in the DM spike density profile normalization or slope translate into different cross-section values that can be probed. Fig. 6 illustrates this dependence for the two types of constraints derived from S2, the 2000–2019 astrometric limit and the stellar-lifetime bound.

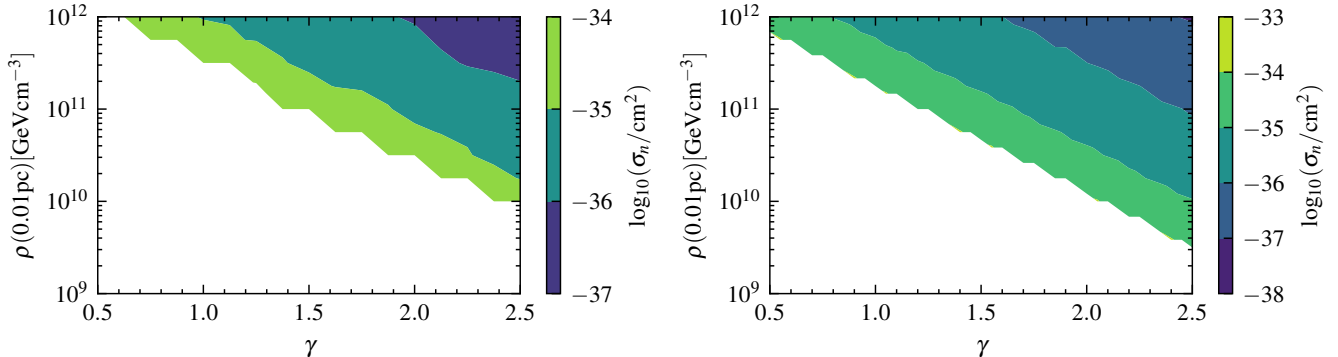


FIG. 6. Minimal DM nucleon-scattering cross-section accessible from S2 observations between 2000 and 2019 (**left**) and from the S2 stellar lifetime constraint (**right**) as a function of the DM spike density normalization and slope. White regions correspond to parameters for which these methods are ineffective.